Available online at www.sciencedirect.com

SciVerse ScienceDirect

Ceramics International 39 (2013) 5893–5899

CERAMICS INTERNATIONAL

www.elsevier.com/locate/ceramint

Boron and zirconium co-doped TiO_2 powders prepared through mechanical ball milling

Tolga Tokmakci[a], Abdullah Ozturk[a], Jongee Park[b,*]

[a]Department of Metallurgical and Materials Engineering, Middle East Technical University, Ankara 06531, Turkey
[b]Department of Metallurgical and Materials Engineering, Atilim University, Ankara 06836, Turkey

Received 29 November 2012; received in revised form 4 January 2013; accepted 5 January 2013
Available online 16 January 2013

Abstract

A titania photocatalyst co-doped with boron and zirconium was prepared by mechanical ball milling. The resulting powder was characterized by XRD, XPS, SEM, and EDS. The photocatalytic performance of the powder was evaluated by degradation of methylene blue (MB) solution under UV illumination. XRD patterns were refined by Rietveld analysis to obtain accurate lattice parameters and positions of the atoms in the crystal structure of the photocatalyst. XRD, XPS, and Rietveld analysis results indicated that mechanical ball milling successfully weaved the dopant elements into the crystal structure and distorted the lattice of TiO_2. Also, SEM micrographs confirmed that mechanical ball milling led to a decrease in average particle size of the photocatalyst. Boron and zirconium co-doped TiO_2 particles exhibited a better visible light response and photocatalytic activity than those of the mono-element doped TiO_2 (i.e. B–TiO_2 and Zr–TiO_2) and undoped TiO_2 particles. The enhanced photocatalytic activity is attributed to the synergistic effects of boron–zirconium co-doping and particle size reduction.

Keywords: A. Mechanical ball milling; Boron; Zirconium; Photocatalysis

1. Introduction

Titanium dioxide (TiO_2) photocatalysis has been an area of great research interest recently, particularly because of its ability to degrade many pollutants from wastes due to its high oxidizing capacity, inexpensiveness, non-toxicity, and photostability [1–3]. Photo-generated electron–hole pairs leaving from light irradiated TiO_2 eliminate a wide variety of harmful organic substances in air or water [4]. Yet, due to its large energy band gap (3.2 eV for anatase), the TiO_2 photocatalysis reaction occurs only under UV light ($\lambda < 388$ nm) irradiation, which accounts for only a small fraction ($\sim 5\%$) of the solar spectrum. In addition, a high degree of electron–hole recombination results in low photo-quantum efficiency, which severely limits the practical applications of TiO_2 as a photocatalyst [5,6]. Lately, doping with a metal [6,7], with a nonmetal [8–10], and co-doping with a metal and a non-metal [11,12] have all been tried for the enhancement of the visible light response and photocatalytic performance of TiO_2. The doping of metal and nonmetal atoms into the TiO_2 lattice decreases the energy band gap, which gives rise to response to the solar illumination [3,9,13].

Woo et al. [14] synthesized Ni^{2+} doped TiO_2 nanostructured powders by mechanical ball milling and reported that Ni^{2+} doped TiO_2 powders showed excellent photo-oxidative ability under visible light irradiation due to the doping effect. Shifu et al. [15] proved that nitrogen and/or carbon doped titania powders with excellent visible-light induced catalytic ability were successfully prepared by mechanical ball milling. Thus, mechanical ball milling could be an effective method for producing metal and/or nonmetal doped photocatalyst TiO_2.

Although there are a few publications [16,17] on the preparation of co-doped photocatalyst TiO_2 with dopants boron and zirconium (through different production routes, including mechanical ball milling), boron and zirconium co-doping on TiO_2 particles by mechanical ball milling has not been thoroughly explored yet.

*Corresponding author. Tel.: +90 312 586 8786; fax: +90 312 586 8091.
E-mail address: jpark@atilim.edu.tr (J. Park).

0272-8842/$ - see front matter © 2013 Elsevier Ltd and Techna Group S.r.l. All rights reserved.
http://dx.doi.org/10.1016/j.ceramint.2013.01.009

The purpose of this study was to improve the visible light response and photocatalytic performance of TiO_2 through co-doping with boron and zirconium by mechanical ball milling. As-prepared powders were characterized by XRD, SEM, EDS and XPS. The degradation of methylene blue solution under UV-light illumination was measured to evaluate photocatalytic performance.

2. Experimental

2.1. Sample preparation

Metatitanate ($TiO(OH)_2$), used as the TiO_2 source, was purchased from Nano Co. Deoinized water was used. All other chemicals used in this study were of analytical grade and used in the as-received form, without further purification.

Initially, various amounts of (0.5, 1.0, 1.5 wt%) Boron (B) doped TiO_2 powders were prepared by mechanical ball milling. These powders were named "B_x–TiO_2", where x represents the B content. In a typical $B_{0.5}$–TiO_2 synthesis experiment, a solution of H_3BO_3 (0.58 g) in water (50 mL) was added dropwise to a stirred solution of $TiO(OH)_2$ (25 g) in water (150 mL). The resulting solution was put in a universal ball mill equipped with a zirconia container and zirconia balls at a milling speed of 450 rpm for 24 h. Then, the as-prepared solution was dried at 105 °C for 15 h and mechanically ground to powder. The resulting dry powder was calcined to 200 °C at the rate of 2 °C min^{-1} and kept at the maximum calcination temperature for 30 min to obtain B-doped TiO_2 samples. $B_{1.0}$–TiO_2 and $B_{1.5}$–TiO_2 were prepared in the same manner.

Zr-doped TiO_2 powders with various amounts of ($y = 0.5$, 1.0, 1.5 wt%) zirconium (Zr) were prepared in a similar manner, replacing the H_3BO_3 solution with a solution of zirconium acetylacetonate ($Zr(C_5H_7O_2)_3$) in EtOH (50 mL). These powders were named as Zr_y–TiO_2, where y represents the Zr content.

Boron–zirconium co-doped TiO_2 powders with a constant amount (0.5 wt%) of B, and various amounts ($z = 0.3$, 0.5, 0.7 wt%) of Zr were prepared by using a mixture of solutions of H_3BO_3 in water and $Zr(C_5H_7O_2)_3$ in EtOH, again following the method described. These powders were named "$B_{0.5}$–Zr_z–TiO_2", where z represents the Zr content.

2.2. Characterization

A D/max-RA X-ray diffractometer (Rigaku-Geigerflex) equipped with Cu target Kα radiation as X-ray source was used to get the XRD patterns in a 2θ range of 20–80° and these patterns were compared with the standard diffraction chart of anatase TiO_2 (JCPDS file number 21-1272). The scanning speed was 2° min^{-1} and accelerating voltage and applied current were 40 kV and 40 mA, respectively. The XRD patterns were also refined using EXPGUI, a graphical user interface for GSAS [18] by the Rietveld refinement method in order to obtain accurate lattice parameters of the samples as well as positions of the atoms in the crystal structure of TiO_2 powders.

To investigate the surface composition and chemical states of the powders, an X-ray photoelectron spectroscope (XPS) was employed with Al Kα radiation. Detailed scans were recorded for B 1s, Zr 3d and Ti 2p. Doped atoms at the surface of TiO_2 were analyzed by means of binding energies obtained from XPS.

A Scanning Electron Microscope (Nova Nanosem 430) was employed to examine surface morphology and estimate the particle size of the prepared powders. Also, EDS was performed to see B and Zr contamination.

2.3. Photocatalytic performance

In order to evaluate photocatalytic performance, methylene blue (MB) solution was chosen as the pollutant model. 200 mL of 10 mg/L MB aqueous solution and 10 mg of powder were added in a self-designed vessel. For the purpose of maintaining a constant photoreaction temperature, the vessel was steeped in a thermostatic circulation bath while the reaction mixture was magnetically stirred. A 100 W Black Ray grade ultra-violet (UV) semiconductor inspection lamp located 10 cm above the vessel was used as a light source. The suspension was stirred for 30 min in the dark for the MB solution to reach adsorption/desorption equilibrium. Each 4 mL suspension was sampled after 30 min and 2 h. A Scinco S-3100 UV–vis single beam spectrophotometer was used to determine the characteristic wavelength ($\lambda = 664$ nm) of MB. The photocatalytic activity is evaluated by [19]

$$\text{degradation ratio } (\%) = [(A0 - A)/A0] \times 100 \quad (1)$$

where $A0$ and A represent absorbance before irradiation and absorbance at radiation time t, respectively.

3. Results and discussion

3.1. XRD patterns of TiO_2 powders

The XRD patterns of as-received TiO_2 powders in undoped and milled form as well as doped and co-doped form are shown in Fig. 1. The XRD analysis of the powders revealed that doped and undoped powders are composed of anatase TiO_2 and did not exhibit any additional phase. No peaks related to B and Zr species were detected in the XRD patterns of powders. This may be because i) the concentration of dopants was so low that XRD was not sufficient for detection or ii) boron and zirconium ions may have been incorporated into the lattice of TiO_2 and occupied some of the titanium lattice sites. A comparison between the XRD patterns of the JCPDS 21-1272 card of anatase TiO_2 and doped and co-doped TiO_2 powders suggests that TiO_2 retained the anatase structure after doping with B and/or Zr ions.

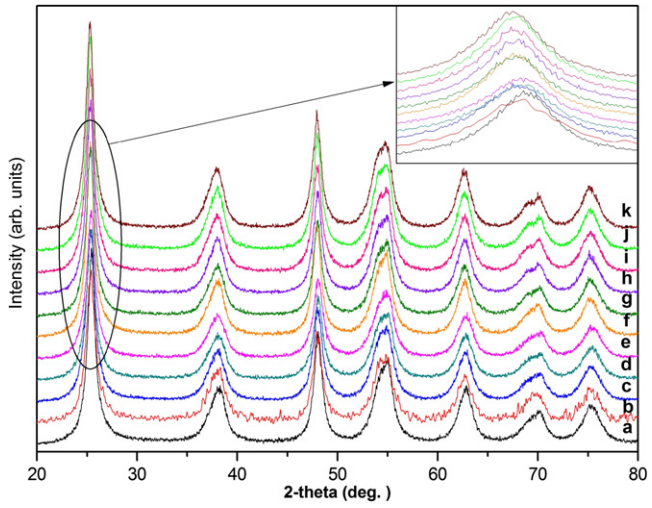

Fig. 1. XRD patterns for (a) unmilled TiO_2, (b) milled TiO_2, (c) $B_{0.5}$–TiO_2, (d) $B_{1.0}$–TiO_2, (e) $B_{1.5}$–TiO_2, (f) $Zr_{0.5}$–TiO_2, (g) $Zr_{1.0}$–TiO_2, (h) $Zr_{1.5}$–TiO_2, (i) $B_{0.5}$–$Zr_{0.3}$–TiO_2, (j) $B_{0.5}$–$Zr_{0.5}$–TiO_2, and (k) $B_{0.5}$–$Zr_{0.7}$–TiO_2.

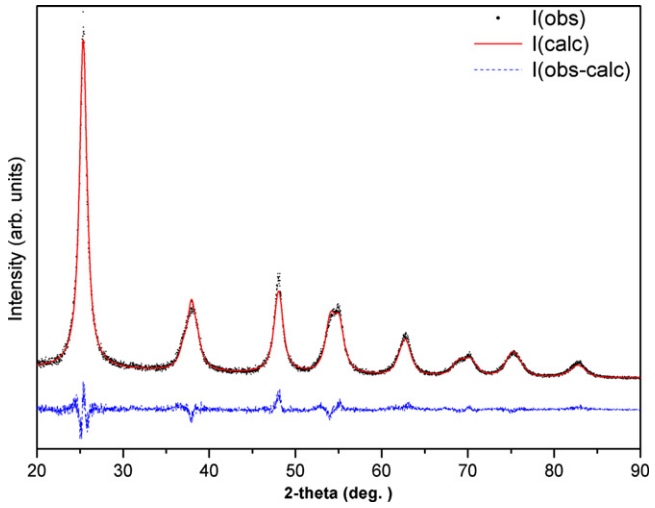

Fig. 2. XRD pattern along with Rietveld refined data for powder $B_{0.5}$–$Zr_{0.3}$–TiO_2. The '•'signs represent experimental points and the solid line represents Rietveld refined data. The dotted line shows the difference between experimental and refined data.

A full-profile refinement was performed to diffraction patterns of undoped TiO_2, $B_{0.5}$–TiO_2, $Zr_{0.5}$–TiO_2, and $B_{0.5}$–$Zr_{0.3}$–TiO_2 powders in order to determine the cell parameters, cell volumes, and atomic positions of B and/or Zr ions in the TiO_2 lattice. A typical well-refined XRD pattern for $B_{0.5}$–$Zr_{0.3}$–TiO_2 powder is shown in Fig. 2. The values of the refinement parameters are summarized in Table 1. The lattice parameters of powders $B_{0.5}$–TiO_2, $Zr_{0.5}$–TiO_2, and $B_{0.5}$–$Zr_{0.3}$–TiO_2 changed due to the integration of B and/or Zr ions into the TiO_2 structure, which resulted in an increase in cell volume as compared with undoped TiO_2. Furthermore, it is clear that dopant atoms shifted the diffraction peaks of (101) crystal plane to lower diffraction angles (Fig. 1, inset). When a comparison is made between the XRD patterns of unmilled TiO_2 and milled TiO_2 powders, apparent peak broadening is observed. It is believed that the mechanical ball milling induced not only grain refinement, but also caused coupling reaction between various dopants and TiO_2 powder. Similar results have been reported by Shifu et al. [15].

The substitution of B^{3+} in the lattice of Ti^{4+} and O^{2-} decreased the cell volume of TiO_2 since the radius of B^{3+} (0.023 nm) is smaller than those of Ti^{4+} (0.068 nm) and O^{2-} (0.132 nm). Thus, it should be expected that diffraction peaks would shift to larger diffraction angles [20]. However, it was consistently observed that diffraction peaks of B doped powders shifted to lower diffraction angles (Fig. 1, inset). The shift of diffraction peaks to lower angles implies that B^{3+} ions entered the lattice of TiO_2 not substitutionally but interstitially. In an interstitial position, the B atom and three close O atoms form a planar structure in a TiO_2 lattice, and the B atom thus adopts sp2 hybridization [21]. This judgment is supported by the fractional atomic positions (Table 2). The B atoms presented in the TiO_2 lattice at different atomic positions (0, 0.75, 0.2679) to Ti (0, 0.75, 0.1250) and O (0, 0.75, 0.3333) without any change in the occupancy values of Ti and O atoms (1.000) in the powder $B_{0.5}$–TiO_2. Also, this new atomic position has been defined by multiplicity of "8" and Wyckoff notation of "*e*" in $I4_1/amd$ space group symmetry [22].

For Zr doping, only the substitution mechanism is active since the lattice spacing of TiO_2 is not sufficient to allow Zr ions with an ionic radius of 0.084 nm to dope into the TiO_2 crystal lattice [23]. The fractional atomic positions of Ti and Zr are identical (0, 0.75, 0.1250) for the powders $B_{0.5}$–TiO_2, $Zr_{0.5}$–TiO_2, and $B_{0.5}$–$Zr_{0.3}$–TiO_2 (Table 2). These findings confirm that Zr atoms tend to enter into the TiO_2 lattice via substitution by Ti atoms. Decrease in Ti occupancy from 1.000 to 0.7495 after incorporation of Zr atoms into the TiO_2 crystal lattice in powder $Zr_{0.5}$–TiO_2 provides further proof of Zr^{4+}–Ti^{4+} substitution. Moreover, the shift of diffraction peaks to smaller diffraction angles in powder $Zr_{0.5}$–TiO_2 is explained by an increase in cell volume of $Zr_{0.5}$–TiO_2 as compared to undoped TiO_2. The cell volume of the TiO_2 lattice increased after Zr doping since the radius of Zr^{4+} is bigger than that of Ti^{4+}, which induced lattice enlargement.

For B and Zr co-doping, all Rietveld analysis results, including occupancy of atoms and fractional atomic positions, are inconsistent with that obtained from only B or only Zr doping. The synergistic effect of intersititial B doping and substitutional Zr doping has had the biggest impact in terms of increase in cell volume of powder $B_{0.5}$–$Zr_{0.3}$–TiO_2 as compared to undoped TiO_2, signifying that co-doping provides the higher distortion in TiO_2 lattice.

3.2. XPS spectra of TiO_2 powders

The XPS spectra of $B_{0.5}$–$Zr_{0.3}$–TiO_2 for B 1s, Zr 3d and Ti 2p are shown in Figs. 3–5, respectively. B and Zr, originated from the dopants during the milling process,

Table 1
Values of the refinement parameters obtained from XRD analysis by employing the Rietveld method.

Refinement parameters	Undoped TiO_2	$B_{0.5}$–TiO2	$Zr_{0.5}$–TiO_2	$B_{0.5}$–$Zr_{0.3}$–TiO_2
Space group	$I4_1/amd$	$I4_1/amd$	$I4_1/amd$	$I4_1/amd$
Ti (occup.)	1.0000	1.0000	0.7495	0.9369
O (occup.)	1.0000	1.0000	1.0000	1.0000
B (occup.)	0.0000	0.2204	0.0000	0.1819
Zr (occup.)	0.0000	0.0000	0.2061	0.0510
$a=b$ (Å)*	3.7921	3.7899	3.7932	3.7976
c (Å)*	9.4879	9.5018	9.4935	9.4904
Volume (Å^3)	136.44	136.48	136.60	136.87
χ^2 (chi^2)**	10.851	5.9360	6.6810	7.2450
*Rp***	7.7500	9.3800	7.7400	6.2300
*Rwp***	12.180	11.020	12.750	11.020

*a, b and c are lattice parameters.
**χ^2, *Rp* and *Rwp* are measures of goodness of the Rietveld fitting.

Table 2
Fractional atomic position of powders $B_{0.5}$–TiO_2, $Zr_{0.5}$–TiO_2, and $B_{0.5}$–$Zr_{0.3}$–TiO_2.

Powder	Ti(x, y, z)	O(x, y,z)	B(x, y, z)	Zr(x, y, z)
$B_{0.5}$–TiO_2	(0, 0.75, 0.1250)	(0, 0.75, 0.3333)	(0, 0.75, 0.2679)	–
$Zr_{0.5}$–TiO_2	(0, 0.75, 0.1250)	(0, 0.75, 0.3333)	–	(0, 0.75, 0.1250)
$B_{0.5}$–$Zr_{0.3}$–TiO_2	(0, 0.75, 0.1250)	(0, 0.75, 0.3333)	(0, 0.75, 0.2987)	(0, 0.75, 0.1250)

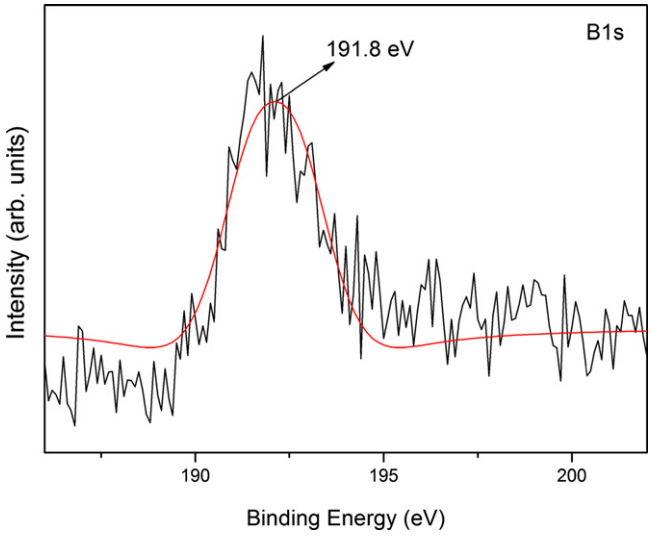

Fig. 3. XPS spectra of powder $B_{0.5}$–$Zr_{0.3}$–TiO_2 for B 1s.

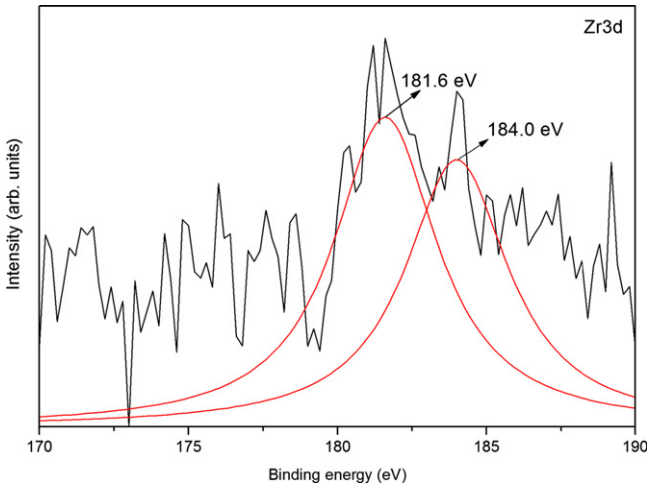

Fig. 4. XPS spectra of powder $B_{0.5}$–$Zr_{0.3}$–TiO_2 for Zr 3d.

were detected in the broad scan XPS spectrum. The binding energy (BE) for B 1s was 191.8 eV. Previous researchers have reported the binding energies (BEs) for B 1s to be 193.6 eV in B_2O_3, 193.0 eV in H_3BO_3, and 187.5 eV in TiB_2 [24–26]. XPS results verified that the B atoms were not bonded by means of a B–Ti–B or B–O–B bond. The BEs for Ti 2p were 458.0 eV and 463.6 eV, which can be attributed to Ti $2p_{3/2}$ and Ti $2p_{1/2}$ of TiO_2, respectively. Mavel et al. [26] reported a BE for Ti $2p_{3/2}$ in TiB_2 of 454.4 eV, which signifies that there was no existence of the compound TiB_2 and B–Ti–B bond (the BEs for Zr 3d were 181.6 eV and 184.0 eV). Bastl et al. [27] reported BEs for Zr 3d of 179.4 eV in ZrH_x, 179.96 eV in Zr_2O, 180.64 eV in ZrO, 182.03 eV in Zr_2O_3, and 183.10 eV in ZrO. These results reveal that Zr–O and Zr–H bonds were not present. The existence of dopant atoms B and Zr in the broad scan XPS spectrum and no formation of any compound including B, Zr, O and Ti other than TiO_2, clearly show that B and Zr atoms weaved into the TiO_2 crystal lattice interstitially and substitutionally, respectively.

3.3. SEM and EDS of TiO_2 powders

Typical SEM images of powders $B_{0.5}$–TiO_2, $Zr_{0.5}$–TiO_2, and $B_{0.5}$–$Zr_{0.3}$–TiO_2 are shown in Fig. 6. SEM examination revealed that the powders were composed of irregularly shaped and agglomerated particles. The average particle size was 30 nm.

The SEM–EDS spectra for powder $B_{0.5}$–$Zr_{0.3}$–TiO_2 shown in Fig. 7 suggest that all the compositions present in the powder are close to the empirical formula of the material. The atomic percentages of O, Ti, B, and Zr are 22.60, 75.48, 0.34, and 1.58, respectively.

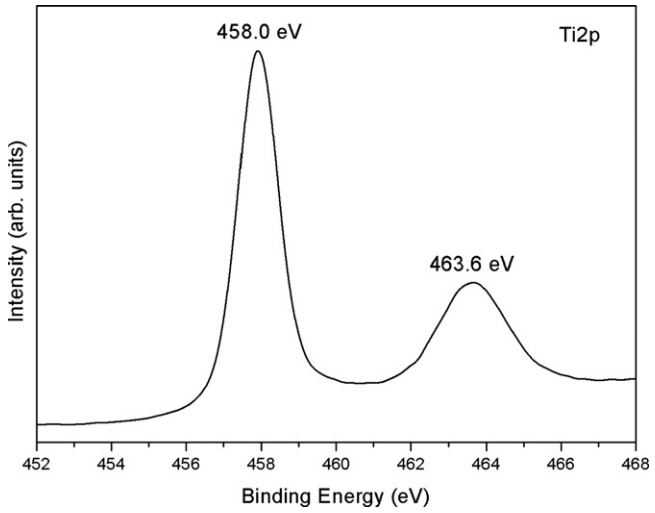

Fig. 5. XPS spectra of powder $B_{0.5}$–$Zr_{0.3}$–TiO_2 for Ti 2p.

3.4. Photocatalytic performance

Photocatalytic performance was evaluated by determining the degradation of methylene blue (MB) solution. Unmilled and milled TiO_2 powders were taken as reference photocatalysts to compare the photocatalytic performance of the doped/co-doped TiO_2 powders. Fig. 8 shows the degradation of MB solution with respect to irradiation time under UV light for unmilled TiO_2, milled TiO_2, B-doped TiO_2, Zr-doped TiO_2, and B–Zr co-doped TiO_2 powders. Milled TiO_2 powder photodegraded 71.70% of the MB, whereas unmilled TiO_2 powder photodegraded only 61.25% of the MB after 2 h of UV irradiation. It has been clarified that the mechanical milling has induced the grain refinement, defect, and lattice distortion which led to an improvement in photocatalytic activity [15]. A small amount (0.5 wt%) of B and Zr doping caused an improvement in photocatalytic performance with regard to the reference photocatalysts. B and Zr co-doped powders displayed better activity for the photodegradation of the MB solution than milled TiO_2, mono-B-doped and mono-Zr-doped TiO_2 powders. $B_{0.5}$–TiO_2, $Zr_{0.5}$–TiO_2, and $B_{0.5}$–$Zr_{0.3}$–TiO_2 powders have given the best individual photocatalytic performance in their groups, implying that an excess of either

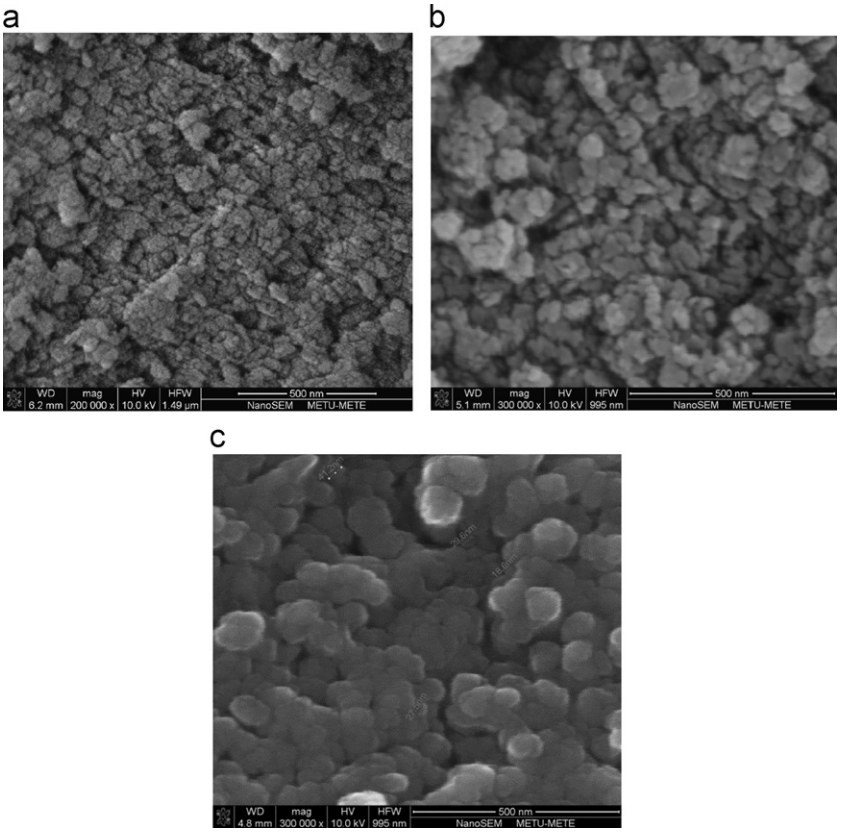

Fig. 6. SEM images of powders of (a) $B_{0.5}$–TiO_2, (b) $Zr_{0.5}$–TiO_2, and (c) $B_{0.5}$–$Zr_{0.3}$–TiO_2.

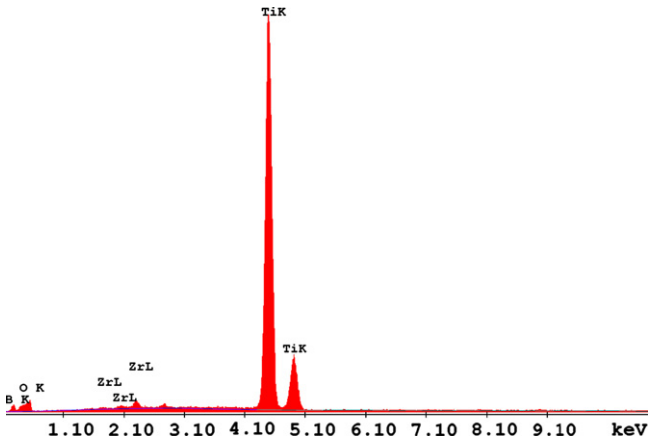

Fig. 7. SEM–EDS of powder $B_{0.5}$–$Zr_{0.3}$–TiO_2.

dopant is not effective in improving photocatalytic performance. The reason for this is not clear to the authors at present and constitutes the subject of another study. Among all of the powders investigated, the best photocatalytic performance was attained with the $B_{0.5}$–$Zr_{0.3}$–TiO_2 powder that photodegraded 91.72% of the MB after 2 h UV irradiation. The photocatalytic performance of $B_{0.5}$–$Zr_{0.3}$–TiO_2 powder was approximately 20% better than that of milled TiO_2 powder. Results suggest that the cooperative effect of B and Zr doping is outstanding in terms of photocatalytic performance. The better photocatalytic activity of $B_{0.5}$–$Zr_{0.3}$–TiO_2 powder is linked to the higher anatase crystallinity, intense light absorption capability in the UV region, and narrower band gap energy.

The improved photocatalytic activity of B and Zr co-doped powders compared to undoped and mono-B and Zr doped TiO_2 powders for the degradation of MB under UV light irradiation could be interpreted as the result of an increase in the quantity of photogenerated charge carriers caused by co-doping with B and Zr. In this case, a greater number of separated photogenerated electrons and holes (e^-/h^+) would be available to participate in the photodegradation process, resulting in better photocatalytic efficiency than that of either undoped or mono-doped TiO_2 powders.

It also worth noting that the better photocatalytic performance of the powders in the order $B_{0.5}$–$Zr_{0.3}$–TiO_2 > $Zr_{0.5}$–TiO_2 > $B_{0.5}$–TiO_2 is consistent with the increase in cell volumes (136.87 $Å^3$ > 136.60 $Å^3$ > 136.48 $Å^3$). Consequently, the extent of distortion in the TiO_2 crystal lattice is directly related to the photocatalytic performance.

4. Conclusions

The boron and zirconium co-doped photocatalyst TiO_2 can be successfully prepared by mechanical ball milling. Boron atoms may be doped intersitially and zirconium atoms substitutionally into the crystal lattice of TiO_2. The incorporation of B and Zr ions into the crystal lattice causes some amount of distortion and increases the cell volume of the TiO_2 lattice structure. B and Zr co-doping provides a higher distortion in the TiO_2 lattice. The extent of distortion in TiO_2 crystal lattice is directly related to photocatalytic performance. The photocatalytic degradation rate of the

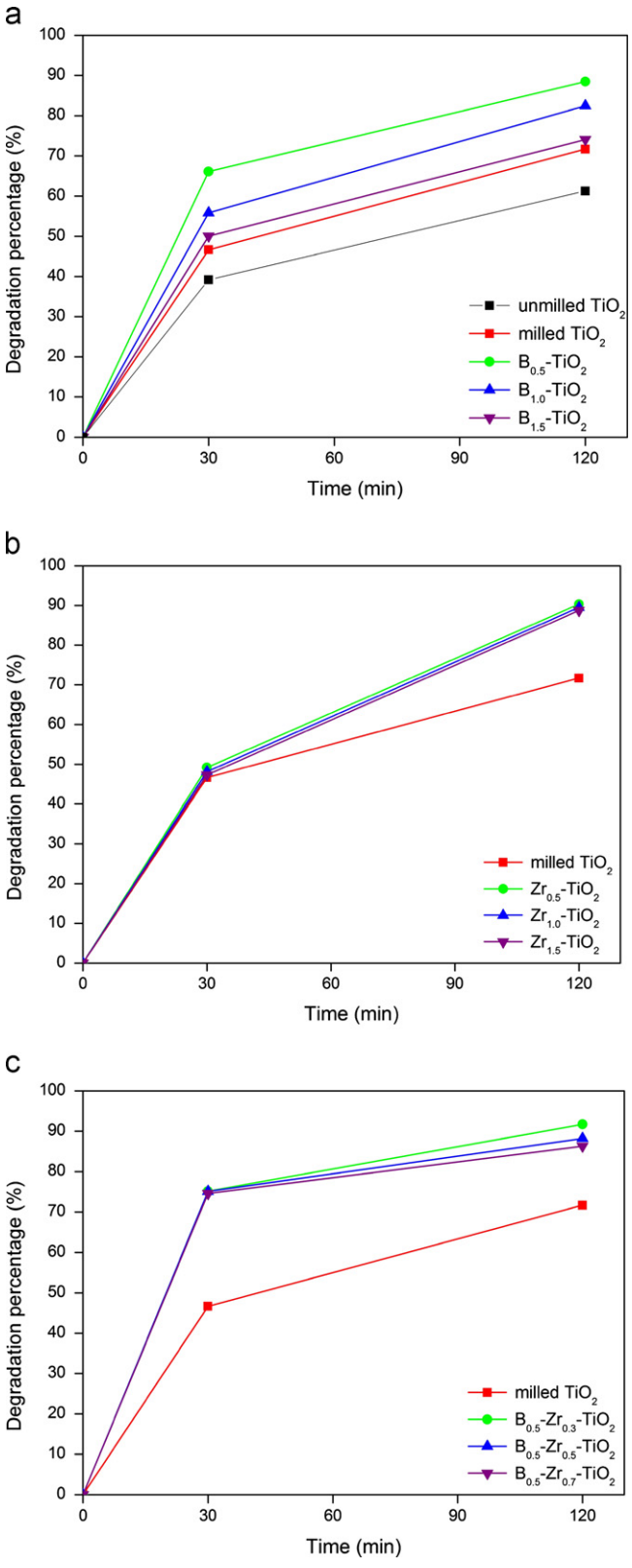

Fig. 8. Degradation of MB solution with time under UV light for powders (a) B–TiO_2, (b) Zr–TiO_2, and (c) B–Zr–TiO_2.

MB solution on TiO_2 powder can be greatly improved by B and/or Zr doping. Compared with undoped TiO_2 powder, B–Zr co-doped TiO_2 powder exhibits a 20% enhancement in photocatalytic performance for the degradation of the MB solution under UV-light illumination. This shows that the synergistic effects of B–Zr co-doping and particle size reduction are responsible for significant improvement in the photocatalytic performance.

Acknowledgments

This work was partially supported by the National Boron Research Institute of Turkey, Project number BOREN-2010. Ç0275.

References

[1] M.R. Hoffmann, S.T. Martin, W. Choi, D.W. Bahnemannt, Chemical Reviews 95 (1995) 69–96.
[2] A. Fujishima, X. Zhang, Comptes Rendus Chimie 9 (2006) 750–760.
[3] R. Asahi, T. Morikawa, T. Ohwaki, K. Aoki, Y. Taga, Science 293 (2001) 269–271.
[4] K. Hashimoto, H. Irie, A. Fujishima, Japanese Journal of Applied Physics 44 (2005) 8269–8285.
[5] X. Cheng, X. Yu, Z. Xing, Applied Surface Science 258 (2012) 7644–7650.
[6] W. Choi, A. Termin, M.R. Hoffmann, Journal of Physical Chemistry 98 (1994) 13669–13679.
[7] B. Babić, J. Gulicovski, Z. Dohčević-Mitrović, D. Bučevac, M. Prekajski, J. Zagorac, B. Matović, Ceramics International 38 (2012) 635–640.
[8] X. Bu, G. Zhang, C. Zhang, Applied Surface Science 258 (2012) 7997–8001.
[9] T. Ohno, M. Akiyoshi, T. Umebayashi, K. Asai, T. Mitsui, M. Matsumura, Applied Catalysis A 265 (2004) 115–121.
[10] M.C. Wang, H.J. Lin, C.H. Wang, H.C. Wu, Ceramics International 38 (2012) 195–200.
[11] Y. Wu, J. Zhang, L. Xiao, F. Chen, Applied Surface Science 256 (2010) 4260–4268.
[12] R. Khan, S.W. Kim, T.J. Kim, C.M. Nam, Materials Chemistry and Physics 112 (2008) 167–172.
[13] S. Yin, M. Komatsu, Q.W. Zhang, R.X. Li, Q. Tang, F. Saito, T. Sato, Chinese Journal of Process Engineering 6 (2006) 3–7.
[14] S.H. Woo, W.W. Kim, S.J. Kim, C.K. Rhee, Materials Science and Engineering A 449-451 (2007) 1151–1154.
[15] C. Shifu, C. Lei, G. Shen, C. Gengyu, Materials Chemistry and Physics 98 (2006) 116–120.
[16] C.H. Wei, X.H. Tang, J.R. Liang, S.Y. Tan, Journal of Environmental Science 19 (2007) 90–96.
[17] N. Venkatachalam, M. Palanichamy, B. Arabindoo, V. Murugesan, Journal of Molecular Catalysis A: Chemical 266 (2007) 158–165.
[18] B.H. Toby, Journal of Applied Crystallography 34 (2001) 210–213.
[19] Q. Ling, J. Sun, Q. Zhou, Applied Surface Science 254 (2008) 3236–3241.
[20] J. Yuan, E. Wang, Y. Chen, W. Yang, J. Yao, Y. Cao, Applied Surface Science 257 (2011) 7335–7342.
[21] H. Geng, S. Yin, X. Yang, Z. Shuai, B. Liu, Journal of Physics: Condensed Matter 18 (2006) 87–96.
[22] T. Hann, International Tables for Crystallography Volume A: Space group 141 (2006) 482–485.
[23] B.M. Reddy, P. Bharali, P. Saikia, G. Thrimurthulu, Y. Yamada, T. Kobayashi, Industrial and Engineering Chemistry Research 48 (2009) 453–462.
[24] D.J. Joyner, D. Hercules, Journal of Chemical Physics 72 (1980) 1095–1108.
[25] J.A. Schreifels, P.C. Maybury, W.E. Swartz Jr., Journal of Catalysis 65 (1980) 195–206.
[26] G. Mavel, J. Escard, P. Costa, J. Castaing, Surface Science 35 (1973) 109–116.
[27] Z. Bastl, A.I. Senkevich, I. Spirovova, V. Vrtilkova, Surface and Interface Analysis 34 (2002) 477–480.